The Crystal Structure of Mouse Exo70 Reveals Unique Features of the Mammalian Exocyst

Brian A. Moore[†], **Howard H Robinson**[§], and **Zhaohui Xu**[†,*]

[†] *Life Sciences Institute and Department of Biological Chemistry, Medical School, University of Michigan, Ann Arbor, MI 48019*

[§] *Biology Department, Brookhaven National Laboratory, Upton, NY 11973*

Abstract

The exocyst is a eukaryotic tethering complex necessary for the fusion of exocytic vesicles with the plasma membrane. Its *in vivo* function is tightly regulated by interactions with multiple small GTPases. Exo70, one of the eight subunits of the exocyst, is important for the localization of the exocyst to the plasma membrane. It interacts with TC10 and Rho3 GTPases in mammals and yeast, respectively, and has recently been shown to bind to the actin-polymerization complex Arp2/3. Here we present the crystal structure of *Mus musculus* Exo70 at 2.25Å resolution. Exo70 is composed of α-helices in a series of right-handed helix-turn-helix motifs organized into a long rod of length 170Å and width 35Å. Although the α-helical organization of this molecule is similar to that in *Saccharomyces cerevisiae* Exo70, major structural differences are observed on the surface of the molecule, at the domain boundaries, and in various loop structures. In particular, the C-terminal domain of *M. musculus* Exo70 adopts a new orientation relative to the N-terminal half not seen in *S. cerevisiae* Exo70 structures. Given the low level of sequence conservation within Exo70, this structure provides new insights into our understanding of many species-specific functions of the exocyst.

Keywords

Crystallography; Membrane Trafficking; Exocytosis; Exocyst; Exo70

INTRODUCTION

Intracellular vesicle delivery depends upon a series of protein complexes working in tandem to transport, tether, and fuse vesicles to specific target membranes. Tethering complexes are thought to mediate the SNARE-dependent fusion of these vesicles to the target membrane at specific sites. In exocytosis, exocytic vesicles are transported from the Golgi apparatus along the cytoskeleton to specific fusion sites on the plasma membrane (PM) by the unconventional myosin Myo2 in yeast[1,2] and others in mammals. The exocyst is a multi-subunit tethering complex involved in exocytosis and receptor recycling[3–6]. It has been identified in most eukaryotes[7] and is composed of eight protein subunits: Sec3, Sec5, Sec6, Sec8, Sec10, Sec15, Exo70, and Exo84[3,8–10]. The exocyst is the first contact between the vesicle and the PM in

exocytosis and is known to regulate exocytosis through interactions with multiple small GTPases in a GTP-dependent manner, including Rho1[11], Rho3[12], Cdc42[13], and Sec4[14] in yeasts; and RalA[15–18], TC10[19], Arf6[5], and Rab11[20] in mammals. Disruption of the exocyst function does not affect the ability of exocytic vesicles to reach the PM, but it does affect the ability of these vesicles to fuse with the PM[21,22].

Exo70 is the 70kDa subunit of the exocyst and its primary sequence is only weakly conserved among Exo70 orthologs (16% identity and 35% similarity between *Mus musculus* and *Saccharomyces cerevisiae*). Within the exocyst, Exo70 is known to interact with Sec6[23,24], Sec8[23,25], and Sec10[23,25]. It also interacts with Sec15 and Exo84 in mammals[24] and Sec5 in yeast[14]. More recently, Arpc1, a subunit of the Arp2/3 complex, has been shown to interact with Exo70, and this interaction is important for actin network reorganization at the PM in both yeast and mammals[26]. Exo70 also mediates interactions between the exocyst and small GTPases, which appears to play a role in the regulation and assembly of the exocyst. Interaction with activated TC10 regulates the presence of exocytic sites at lipid rafts in insulin-stimulated glucose transport in mammals[19,27]. In yeast, interaction with activated Rho3 controls the fusion of exocytic vesicles with the PM[12,28] and may also be important in demarcation of exocytic sites[29]. Despite some overlapping functions, however, interaction with these small GTPases occurs at two separate sites on Exo70[19,23], suggesting that the functional organization of Exo70 may not be entirely conserved. While the recently reported structures of *S. cerevisiae* Exo70 (*Sc*Exo70)[23,30] have been used as a general model to understand the structure and function relationship of all Exo70 proteins, it is essential to obtain high-resolution structural information of mammalian Exo70 in order to address questions specific to mammalian exocytosis.

Here we report the crystal structure of *M. musculus* Exo70 (*Mm*Exo70) at 2.25Å resolution. Comparison to the structure of *Sc*Exo70 reveals that while the overall fold of the protein is conserved, there is significant structural reorganization within the molecule that results in the reorientation of the C-terminal domain relative to the rest of the molecule. In addition, loops connecting secondary structural elements show significant differences in length and conformation. This, combined with a general lack of primary sequence conservation, results in the alteration of the molecule's surface properties. The observed structural similarity and differences are consistent with the function of Exo70 as an exocyst subunit that interacts with different sets of effector molecules in different organisms. The structure of *Mm*Exo70 is the first structure of a mammalian exocyst subunit and makes Exo70 the first exocyst subunit with structural information available in more than one organism.

RESULTS AND DISCUSSION

Structure determination

To obtain diffraction-quality crystals of *Mm*Exo70, purified full-length protein was subjected to limited proteolysis by subtilisin, which identified a major fragment containing a deletion of the N-terminal 84 residues of the molecule. This fragment (residues 85–653) was crystallized in the P3$_2$21 space group with unit cell dimensions of a = b = 61.5Å, c = 294.7Å and one molecule in the asymmetric unit. The structure was determined by the multi-wavelength anomalous diffraction (MAD) method using crystals grown from L-selenomethionine-substituted protein. The final model was refined to a resolution of 2.25Å with an R-factor of 23.5% and an R$_{free}$ of 28.5% (Table 1), which contains residues 85–179, 188–241, 275–446, 455–652, and 170 water molecules. There is no clear electron density observable for residues 180–187, 242–274, 447–454, and 651–653. These residues are presumably disordered. Of all residues in the structure, 92.8% are found in the most favored regions of the Ramachandran plot[31], while the rest are found in either the additionally allowed (6.5%) or the generously allowed (0.6%) regions.

Structural organization of *Mm*Exo70

*Mm*Exo70 is composed of nineteen α-helices (H1-H19) connected by loops of varying lengths (L_{1-2}-L_{18-19}; numbers identify adjoining α-helices) organized into three distinct domains to form a 170 Å-long, 35 Å-wide rod-shaped molecule (Figure 1a, 2). The N domain is composed of residues 85–393, including H1-H9 and the first half of H10. These α-helices are organized into a series of right-handed helix-turn-helix motifs with a slight super-helical twist that extends nearly 100Å. H4 is the shortest helix in this domain and is an exception to the helix-turn-helix motif as it is perpendicular to the other α-helices. Most of the loops in this domain are short (2–5 residues) except for L_{4-5}, a partially disordered loop of sixteen-residues, and L_{6-7}, which contains up to 33 disordered residues and is predicted to be largely unstructured[32]. The M domain is composed of residues 394–538, including the second half of H10, H11-H15, and the first half of H16. These helices are organized into a 55Å-long five-helix bundle that maintains the right-handed helix-turn-helix motif. The long axis of this domain is canted about 40° from the long axis of the full molecule. H12 and H15 are two short helices that are not part of the α-helical bundle structure, as they both closely follow the preceding helix with an approximate 90° turn. The loops of the M domain are short except for L_{10-11} and L_{12-13}, which are 15 and 10 residues long, respectively, with most of L_{12-13} being disordered. The C domain is composed of residues 539–650, including the second half of H16 and H17–H19. These helices are organized into a 55Å-long four-helix bundle that continues the right-handed helix-turn-helix motif. The boundary between the M and C domains is defined by a kink in H16 that orients this domain along the long axis of the molecule.

The interface between the N and M domains, consisting of residues from H8-H9 and H10-H12, appears as a thin "neck" with a buried surface area of about 740Å^2 (Figure 3a). It is composed of two small hydrophobic patches that each contains a cluster of mostly aromatic residues and a few surrounding water-mediated hydrogen bonds. The first hydrophobic patch includes Phe351 (H9) packing against Phe434 (H12). The second hydrophobic patch, separated by 6Å from the first, consists of Phe344 (L_{8-9}) packing against Phe397 (H10) and Phe427 (H11). The hydrogen bonds involve the main chain carbonyl group of Ile339 (H8) and the side chain of His342 (L_{8-9}) interacting with the side chain of Asn400 (H10), the side chain of Arg355 (H9) interacting with the main chain carbonyl group of Asp433 (H11) and the side chain of Glu436 (H12), and the side chain of Glu387 (H10) interacting with the side chain of Gln445 (H12).

The interface between the M and C domains primarily involves L_{10-11}, H14, and H16 packing against H17-H18 and buries about 755Å^2 of surface area (Figure 3b). Many hydrophobic residues on H14 and H16 interact with residues on H17-H18, composing the core of this interface. In addition, a number of hydrogen bond interactions also stabilize the domain interface. These include main chain interaction between the carbonyl group of Asp414 (L_{10-11}) and the amide group of Ala592 (L_{17-18}), side chain interaction between His496 (H14) and Gln598 (H18), side chain interaction between Asn500 (H14) and Asp595 (L_{17-18}), dual side chain interactions between Gln588 (H17) and Tyr537/Ser540 (H16), and water mediated dual hydrogen bonds between the side chain of Asp497 (H14) and the main chain carbonyl group of Ala592/the main chain amide group of Asp595 (L_{17-18}). Interestingly, L_{10-11} and L_{17-18} are parallel to one another for a length of 11Å but interact only through the one main chain hydrogen bond mentioned above.

Conserved residues of Exo70

The low level of primary sequence conservation among Exo70 orthologs makes previous sequence alignment, and therefore identification of conserved residues, unreliable. The structure of *Mm*Exo70 enables, for the first time, structure-based sequence alignment to examine the role of conserved residues in Exo70 (Figure 2). For structural comparison with *Sc*Exo70 throughout this study, a crystal structure of *Sc*Exo70 determined in our own lab was

used (see supplementary information). Briefly, this *Sc*Exo70 structure was determined to a resolution of 2.1 Å, which is similar to the published $P2_12_12_1$ form[23] and much higher than the published C2 form[30]. The overall structure is nearly identical to that of the $P2_12_12_1$ form, with a root-mean square distance (rmsd) of 0.4 Å for 532 C_α atoms. Our structure, however, is the most complete *Sc* Exo70 structure available, including seventeen additional residues not present in the $P2_12_12_1$ form and twenty-six additional residues not present in the C2 form.

Structural alignment reveals two regions with clusters of highly conserved residues. The first region is concentrated on L_{10-11} and H11 (Figure 4a). Pro412 is located at the start of a tight turn within L_{10-11} and is likely to be important for this structural feature. Asp414 is located at the end of the turn initiated by Pro412 and its side chain forms a hydrogen bond with the main chain amide of Thr416, possibly stabilizing this turn. As mentioned earlier, the main chain carbonyl group of Asp414 forms a hydrogen bond with the amide group of Ala592 on L_{17-18}. This interaction is possibly stabilized by the side chain interactions of Asp414. Asp595 is located at the end of L_{17-18} and forms a hydrogen bond with the amide group of Glu597 on H18, possibly stabilizing the conformation of this loop. All of these interactions, except the main chain hydrogen bond between Asp414 and Ala592, appear to be conserved in the *Sc*Exo70 structure, suggesting that they are structurally important in supporting this part of the structure. Glu419 is the first residue of H11 and is completely exposed to solvent. The reason for its conservation is not clear but it could be involved in a conserved interaction. It is 12Å away from Asp414 and more than 22Å away from Asp595, the closest conserved surface-exposed charged residues. Finally, Thr421 on H11 forms a hydrogen bond with Asn498 on H14, which acts as a pivot point to allow rearrangement within the M domain (see below).

The second conserved region is a large (almost 400Å^2), mostly hydrophilic surface patch found on H17, H19, and L_{18-19} (Figure 4b). Residues participating in this patch include Lys565, Arg567, Gln568, Lys571, Glu572, Glu582, Glu583 (H17), Lys628, Asn629, Lys632, Tyr633, Ile634, Lys635, Tyr636 (L_{18-19}), Gln640, and Met644 (H19). Completely conserved residues appear mostly surrounded by similarly conserved residues. At least a portion of this region has been recently shown to interact with Arpc1 of the Arp2/3 complex. Mutation of Lys571 and Glu572, or Lys628, Asn629, and Pro630, abolishes the ability of Exo70 to interact with Arpc1[26]. Presumably, all conserved residues on the surface of the C domain either directly interact with Arpc1 or stabilize the local structure. The hydrophobic core of the four-helix bundle is also well conserved and highly aromatic, contributing to the stability of this domain.

Structural Comparison to *Sc*Exo70

*Mm*Exo70 has an overall fold similar to *Sc*Exo70[23,30] (Figure 5a). Each of the nineteen α-helices of *Mm*Exo70 corresponds closely to one of the nineteen α-helices of *Sc*Exo70[23], although the structural differences are significant enough that attempts to determine the *Mm*Exo70 structure by molecular replacement using *Sc*Exo70 as a search model were not successful. Both molecules take the shape of a rod with similar dimensions[23,30]. The rod of *Sc*Exo70 is somewhat more curved and twisted than *Mm*Exo70. This curvature appears to originate primarily from the packing of helices H3-H5 against H6-H7, adding to the super-helical twist of the N domain, and from the packing of H11 and H13 against H14-H16 in the M domain, resulting in the twisting of the C domain away from the long axis of the molecule.

The most notable difference between the two structures lies in the relative orientation of the C-terminal portion of the molecule to the N-terminal portion (Figure 5a). This originates from changes in the helical packing within the M domain. In support of this, the rmsd of the full *Mm*Exo70 and *Sc*Exo70 structures is 7.0Å for 481 C_α atoms, while the rmsd of H1-H13 is 3.6Å for 327 C_α atoms and the rmsd of H14-H19 is 2.9Å for 157 C_α atoms. Structural alignment of *Mm*Exo70 with *Sc*Exo70 based on H10-H13 reveals that H14-H16 adopts a conformation in which H14 and H16 are rotated 18.9° and 24.7°, respectively, between structures (Figure 5b).

This alignment also reveals that the conformational change between the two halves of the molecule appears to pivot about Asn498 (H14), which forms a hydrogen bond with Thr421 (H11). Both of these residues are completely conserved and appear in a similar location in *Sc*Exo70, suggesting that this interaction is important to the internal packing of the M domain.

We argue that this conformational difference in the M domain between *Mm*Exo70 and *Sc*Exo70 is not a reflection of structural flexibility within the M domain. Rather, it suggests inherent structural differences between the two molecules. The thermal factors in this region are comparable to the rest of the molecule. Most importantly, the same conformation is observed in this region in all six independently determined ScExo70 structures[23,30] (The C2 ScExo70 crystal form contains four molecules in the asymmetric unit). Furthermore, the *Mm*Exo70 conformation is stabilized by the previously mentioned interactions between M domain $L_{10–11}$ and C domain $L_{17–18}$ (Figure 5c). This interaction represents the major structural difference in an otherwise well-conserved region. Interestingly, the parallel organization of these loops is also observed in *Sc*Exo70 structures, although residues of these loops are separated for more than 4Å (Figure 5d). In comparison, the *Sc*Exo70 conformation is stabilized by interactions of $L_{12–13}$ and $L_{13–14}$ with H10, H13, and H16. The length of $L_{13–14}$ may contribute to the observed conformational differences as well. The tight turn of the three-residue $L_{13–14}$ in *Mm*Exo70 puts spatial constraints on the location of H14 while the eighteen-residue *Sc*Exo70 $L_{13–14}$ grants more freedom to H14. Our structure-based sequence alignment reveals that *Schizosaccharomyces pombe* and higher eukaryotes have a nearly uniformly short $L_{13–14}$ (Figure 2), suggesting that these organisms may share the same M domain packing and C domain orientation as observed in *Mm*Exo70.

Conformational differences are also observed at the interface between N and M domains. Major structural flexibility has been described for this interface in *Sc*Exo70[30], which contains a similarly thin "neck" with almost 30% less buried surface area ($580Å^2$ compared to $740Å^2$ in *Mm*Exo70)[30] and is composed of only one hydrophobic patch and no hydrogen bonds. Phe306 (H9), Tyr385 ($L_{11–12}$), Phe303 (H9), Phe345 (H10), and Phe382 (H11) in *Sc*Exo70 are structurally equivalent to Phe351 (H9), Phe434 (H12), Phe344 (H9), Phe397 (H10), and Phe427 (H11) in *Mm*Exo70 (Figure 3a). In addition, *Sc*Exo70 H10 is kinked at the domain boundary whereas no apparent kink is seen in *Mm*Exo70 H10, although this does not appear to affect the spatial relationship between the N and M domains or the orientation of the M domain. Currently, there is no evidence to suggest that a similar degree of flexibility also exists at the same domain in *Mm*Exo70, and the increased surface area and number of interactions would argue that it is more stable than in *Sc*Exo70.

Differences in surface electrostatic potential

*Sc*Exo70 has been previously noted for the polarity of its surface electrostatic potential[23,30]. Its N-terminus is strongly electronegative, resulting from an electronegative patch composed mostly of residues from H2, H3 and H5 (Figure 6a). Its C-terminus is primarily electropositive, resulting mostly from residues on $L_{10–11}$, H11, $L_{13–14}$, H14, and H16-H19. This polarity is not observed in *Mm*Exo70 (Figure 6b). The N-terminus lacks the strong electronegative patch, and the C-terminus retains only a small electropositive patch at the extreme tip of the molecule. Despite this difference, the C-terminal basic patch remains a conserved feature on the surface of the molecule. In *Mm*Exo70 it is composed of Lys561, Arg563, Lys565, Arg567, Lys571, Lys575, Lys628, Lys632, and Lys635. All of these residues except Lys561, Arg563, and Lys575 are conserved, suggesting a common biological function. Interestingly, Lys571 and Lys628 have been implicated in Arpc1 interaction[26]. The middle of *Mm*Exo70 has an overall electronegative potential that contrasts with the mixed potential of *Sc*Exo70 in this region. Residues primarily from H4, $L_{4–5}$, H7, H9-H12, H14-H15, $L_{17–18}$ and H18 contribute to this patch. Only a few small regions remain unchanged between the two structures. H6, $L_{16–17}$ and

L_{18-19} compose two electropositive patches while H7 and H9, and H14-H15 compose two electronegative pockets. Therefore, it appears that Exo70 has highly variable surface electrostatic properties suggesting great variability in Exo70-mediated protein-protein interactions.

Similarity to other structures

It has been noted that the N domain of ScExo70[23], the C-terminal domain of *S. cerevisiae* Exo84[23], the C-terminal domain of *S. cerevisiae* Sec6 (ScSec6)[33] and the C-terminal domain of *Drosophila melanogaster* Sec15 (DmSec15)[34] each share a similar fold[33,35]. Not surprisingly, the N domain of MmExo70 also contains this structural feature. A search of the RCSB Protein Data Bank[36] for other proteins with a fold similar to the MmExo70 N domain using the DALI server[37] also identifies the cargo-binding domain of *S. cerevisiae* Myo2 (ScMyo2), a Myosin V motor protein[38] (Figure 7). This is the first instance of this fold appearing in a protein outside of the exocyst complex. The cargo-binding domain of ScMyo2 is located at the C-terminus of the molecule and contains an additional three-helix bundle at its C terminus, similar to ScSec6 and possibly DmSec15[35]. Notably, Rho3 regulates the functions of ScMyo2 and ScExo70, and the interaction of ScMyo2 with Rho3 results in exocytic vesicle delivery that functions alongside exocytosis[12,28]. We also note that of the five proteins now known to contain this fold, Exo70 is unique in having this domain at its N terminus. The function of this fold remains unclear despite its presence in these structures.

TC10 binding

The structure of MmExo70 may reveal details important to understanding the interaction of mammalian Exo70 with small GTPase TC10 that are not available from that of ScExo70. In *H. sapiens* Exo70, residues 1–384 interact with TC10 while affinity is reduced with residues 1–99 and 100–384 individually[19]. The simplest explanation is that the site of interaction with TC10 spans both of these regions. The first 99 residues of MmExo70 extend nearly to the end of H1. Due to a lack of structural information for the first 84 residues of MmExo70, it is unclear how it might be involved in TC10 interaction, although secondary structure prediction suggests that these missing residues may also adopt a similar helix-turn-helix motif as observed in the rest of the molecule[32]. Residues 100–384 contain L_{4-5} and L_{6-7}, both of which are longer in MmExo70 than in ScExo70. These significant structural differences could play important roles in mediating species-specific interactions with TC10, although it is equally possible that the strikingly different surface composition between these molecules could also play an important role.

Conclusion

The structure of MmExo70 reveals that, despite the conservation of the overall fold of Exo70, especially of the N domain that has structural similarity to other proteins involved in exocytosis, there are several major structural reorganizations that result in a different overall shape of the molecule. Packing within the M domain is altered and positions the C domain along the long axis of the molecule. A larger buried surface area and additional interactions add to the stability of the flexible hinge between N and M domains of ScExo70. A lack of sequence conservation for surface residues results in a drastic change in the surface electrostatic potential of the molecule. These differences in Exo70 structure are important to our understanding of many species-specific functions of the exocyst as more is learned about this fascinating molecular machinery.

MATERIALS AND METHODS

*Mm*Exo70 expression and purification

The *Mm*Exo70$_{\Delta 84}$ gene (coding for residues 85–653) was amplified from *M. musculus* cDNA (provided by A. Saltiel) by PCR and subcloned into the pSJ7 vector, a derivative of pET43a (Novagen). The native protein was expressed in *Escherichia coli* BL21(DE3) strain containing the expression plasmid at 16°C in LB media, and the L-Selenomethionine variant protein was expressed in *Escherichia coli* B834(DE3) strain containing the expression plasmid at 16°C in L-Selenomethionine-containing minimal media. Cells were induced with 0.4mM IPTG (Calbiochem) and protein purification was carried out at 4°C. Cell pellets were lysed by sonication in buffer A (50mM Tris pH8.0, 300mM NaCl, 5mM β-mercaptoethanol, 10μg/ml PMSF), and soluble material was passed over a Ni^{2+}-NTA column and eluted with a linear gradient of buffer B (buffer A with 250mM imidazole). The N-terminal NusA-His-tag was removed by proteolysis with TEV protease during dialysis against dialysis buffer (50mM Tris pH8.0, 100mM NaCl, 5mM β-mercaptoethanol, 10μg/ml PMSF). TEV protease and the tag were removed by passage over a second Ni^{2+}-NTA column. *Mm*Exo70 was further purified on a SourceQ column, loaded in buffer C (50mM Tris pH8.0, 1mM dithiothreitol) and eluted with a linear gradient of buffer D (buffer C with 1M NaCl). Purified protein was stored in crystallization buffer (50mM Tris pH8.0, 100mM NaCl, 1mM Tris[2-carboxyethyl]phosphine) at a concentration of 14.5mg/mL (native) or 13.5mg/mL (L-selenomethionine variant).

*Mm*Exo70 crystallization and data collection

Native or L-Selenomethionine variant crystals appeared in 1–2 days and reached full size in 7–10 days at 20°C using the sitting drop method. Equal volumes of protein and precipitant (100mM HEPES pH7.5, 10% ethylene glycol, 5% PEG8000, 10mM MgCl$_2$) were mixed in a 4μL drop and equilibrated over 500μL of well solution (100mM HEPES pH7.5, 10% ethylene glycol, 8% PEG8000). Streak seeding was performed to improve the quality of crystals. Formation of a sticky film with time necessitated prompt harvesting. Crystals were washed in cryo-solution (100mM HEPES pH7.5, 30% ethylene glycol, 10% PEG8000, 10mM MgCl$_2$) before being flash cooled in liquid nitrogen. Native and MAD data were collected at beamline 23-D at the Advanced Photon Source and were processed using HKL2000[39].

*Mm*Exo70 refinement and model building

Experimental phases were obtained using the multi-wavelength anomalous dispersion (MAD) method[40]. Initial heavy atom sites were found using CNS[41] and confirmed using Shake-N-Bake[42]. Refinement of the heavy atom sites was carried out using autoSHARP[43], and ten of the expected eleven selenium sites in the monomer were found (the missing selenium site is located in a disordered portion of the molecule). MAD phases were calculated, solvent flattening was performed, and the initial model was built using autoSHARP. The remainder of the model was built based on the locations of known selenium atoms using O[44], and all refinement procedures were carried out using CNS. Initial refinement consisted of several iterations of simulated annealing by the maximum likelihood target function using amplitudes and phase probability distribution (MLHL), grouped B factor refinement, and model rebuilding using O. This was done using data from the peak wavelength of the MAD data set. Further refinement was done against the native data set to its limiting resolution of 2.25Å. This consisted of iterations of simulated annealing by the maximum likelihood target function using amplitudes, individual B factor refinement, and model building using O. 3F$_o$-2F$_c$ and F$_o$-F$_c$ maps were calculated to aid model building and water placement. The final model consists of residues 85–179, 188–241, 275–446, 455–652, and 170 water molecules.

Figure preparation

Figures 1, 3, 4, 5, and 7 were produced with MacPyMOL (http://www.pymol.org). The sequence alignment shown in Figure 2 is based on structural alignment of *Mm*Exo70 with *Sc*Exo70. Both structures were broken into a series of overlapping three-helix fragments, which were aligned by the DALI server[45]. The sequences of Exo70 from *Candida albicans*, *S. pombe*, *Caenorhabditis elegans*, *D. melanogaster*, and *H. sapiens* were aligned with the *Mm*Exo70/*Sc*Exo70 alignment based on Clustal W[46]. Residues invariable in six of these seven species were considered completely conserved. Residues that always appear as a particular residue type in six of these seven species were considered similarly conserved. Figure 6 was produced using the adaptive Poisson-Boltzmann solver[47] in the APBS Tools plug-in for PyMOL (www.umich.edu/~mlerner/Pymol). All missing side chains, but not completely missing residues, were modeled in a rotamer allowed by the surrounding structure for this calculation. Structural alignment in Figures 5, 6, and 7 were performed using the DALI server or PyMOL.

Protein Data Bank accession number

Atomic coordinates and structure factors have been deposited in the RCSB Protein Data Bank with accession code 2PFT for *Mm*Exo70 and 2PFV for *Sc*Exo70.

Supplementary Material

Refer to Web version on PubMed Central for supplementary material.

Acknowledgments

References

1. Govindan B, Bowser R, Novick P. The role of Myo2, a yeast class V myosin, in vesicular transport. J Cell Biol 1995;128:1055–1068. [PubMed: 7896871]

2. Johnston GC, Prendergast JA, Singer RA. The Saccharomyces cerevisiae MYO2 gene encodes an essential myosin for vectorial transport of vesicles. J Cell Biol 1991;113:539–551. [PubMed: 2016335]

3. TerBush DR, Maurice T, Roth D, Novick P. The Exocyst is a multiprotein complex required for exocytosis in Saccharomyces cerevisiae. Embo J 1996;15:6483–6494. [PubMed: 8978675]

4. Folsch H, Pypaert M, Maday S, Pelletier L, Mellman I. The AP-1A and AP-1B clathrin adaptor complexes define biochemically and functionally distinct membrane domains. J Cell Biol 2003;163:351–362. [PubMed: 14581457]

5. Prigent M, Dubois T, Raposo G, Derrien V, Tenza D, Rosse C, Camonis J, Chavrier P. ARF6 controls post-endocytic recycling through its downstream exocyst complex effector. J Cell Biol 2003;163:1111–1121. [PubMed: 14662749]

6. Ang AL, Taguchi T, Francis S, Folsch H, Murrells LJ, Pypaert M, Warren G, Mellman I. Recycling endosomes can serve as intermediates during transport from the Golgi to the plasma membrane of MDCK cells. J Cell Biol 2004;167:531–543. [PubMed: 15534004]

7. Koumandou VL, Dacks JB, Coulson RM, Field MC. Control systems for membrane fusion in the ancestral eukaryote; evolution of tethering complexes and SM proteins. BMC Evol Biol 2007;7:29. [PubMed: 17319956]

8. Guo W, Grant A, Novick P. Exo84p is an exocyst protein essential for secretion. J Biol Chem 1999;274:23558–23564. [PubMed: 10438536]

9. Hsu SC, Ting AE, Hazuka CD, Davanger S, Kenny JW, Kee Y, Scheller RH. The mammalian brain rsec6/8 complex. Neuron 1996;17:1209–1219. [PubMed: 8982167]

10. Kee Y, Yoo JS, Hazuka CD, Peterson KE, Hsu SC, Scheller RH. Subunit structure of the mammalian exocyst complex. Proc Natl Acad Sci U S A 1997;94:14438–14443. [PubMed: 9405631]

11. Guo W, Tamanoi F, Novick P. Spatial regulation of the exocyst complex by Rho1 GTPase. Nat Cell Biol 2001;3:353–360. [PubMed: 11283608]

12. Robinson NG, Guo L, Imai J, Toh EA, Matsui Y, Tamanoi F. Rho3 of Saccharomyces cerevisiae, which regulates the actin cytoskeleton and exocytosis, is a GTPase which interacts with Myo2 and Exo70. Mol Cell Biol 1999;19:3580–3587. [PubMed: 10207081]

13. Zhang X, Bi E, Novick P, Du L, Kozminski KG, Lipschutz JH, Guo W. Cdc42 interacts with the exocyst and regulates polarized secretion. J Biol Chem 2001;276:46745–46750. [PubMed: 11595741]

14. Guo W, Roth D, Walch-Solimena C, Novick P. The exocyst is an effector for Sec4p, targeting secretory vesicles to sites of exocytosis. Embo J 1999;18:1071–1080. [PubMed: 10022848]

15. Jin R, Junutula JR, Matern HT, Ervin KE, Scheller RH, Brunger AT. Exo84 and Sec5 are competitive regulatory Sec6/8 effectors to the RalA GTPase. Embo J 2005;24:2064–2074. [PubMed: 15920473]

16. Moskalenko S, Henry DO, Rosse C, Mirey G, Camonis JH, White MA. The exocyst is a Ral effector complex. Nat Cell Biol 2002;4:66–72. [PubMed: 11740492]

17. Moskalenko S, Tong C, Rosse C, Mirey G, Formstecher E, Daviet L, Camonis J, White MA. Ral GTPases regulate exocyst assembly through dual subunit interactions. J Biol Chem 2003;278:51743–51748. [PubMed: 14525976]

18. Sugihara K, Asano S, Tanaka K, Iwamatsu A, Okawa K, Ohta Y. The exocyst complex binds the small GTPase RalA to mediate filopodia formation. Nat Cell Biol 2002;4:73–78. [PubMed: 11744922]

19. Inoue M, Chang L, Hwang J, Chiang SH, Saltiel AR. The exocyst complex is required for targeting of Glut4 to the plasma membrane by insulin. Nature 2003;422:629–633. [PubMed: 12687004]

20. Zhang XM, Ellis S, Sriratana A, Mitchell CA, Rowe T. Sec15 is an effector for the Rab11 GTPase in mammalian cells. J Biol Chem 2004;279:43027–43034. [PubMed: 15292201]

21. Grote E, Carr CM, Novick PJ. Ordering the final events in yeast exocytosis. J Cell Biol 2000;151:439–452. [PubMed: 11038189]

22. Walch-Solimena C, Collins RN, Novick PJ. Sec2p mediates nucleotide exchange on Sec4p and is involved in polarized delivery of post-Golgi vesicles. J Cell Biol 1997;137:1495–1509. [PubMed: 9199166]

23. Dong G, Hutagalung AH, Fu C, Novick P, Reinisch KM. The structures of exocyst subunit Exo70p and the Exo84p C-terminal domains reveal a common motif. Nat Struct Mol Biol 2005;12:1094–1100. [PubMed: 16249794]

24. Matern HT, Yeaman C, Nelson WJ, Scheller RH. The Sec6/8 complex in mammalian cells: characterization of mammalian Sec3, subunit interactions, and expression of subunits in polarized cells. Proc Natl Acad Sci U S A 2001;98:9648–9653. [PubMed: 11493706]

25. Vega IE, Hsu SC. The exocyst complex associates with microtubules to mediate vesicle targeting and neurite outgrowth. J Neurosci 2001;21:3839–3848. [PubMed: 11356872]

26. Zuo X, Zhang J, Zhang Y, Hsu SC, Zhou D, Guo W. Exo70 interacts with the Arp2/3 complex and regulates cell migration. Nat Cell Biol 2006;8:1383–1388. [PubMed: 17086175]

27. Inoue M, Chiang SH, Chang L, Chen XW, Saltiel AR. Compartmentalization of the exocyst complex in lipid rafts controls Glut4 vesicle tethering. Mol Biol Cell 2006;17:2303–2311. [PubMed: 16525015]

28. Adamo JE, Rossi G, Brennwald P. The Rho GTPase Rho3 has a direct role in exocytosis that is distinct from its role in actin polarity. Mol Biol Cell 1999;10:4121–4133. [PubMed: 10588647]

29. Boyd C, Hughes T, Pypaert M, Novick P. Vesicles carry most exocyst subunits to exocytic sites marked by the remaining two subunits, Sec3p and Exo70p. J Cell Biol 2004;167:889–901. [PubMed: 15583031]

30. Hamburger ZA, Hamburger AE, West AP Jr, Weis WI. Crystal structure of the S. cerevisiae exocyst component Exo70p. J Mol Biol 2006;356:9–21. [PubMed: 16359701]

31. Ramakrishnan C, Ramachandran GN. Stereochemical criteria for polypeptide and protein chain conformations. II. Allowed conformations for a pair of peptide units. Biophysical Journal 1965;5:909–933. [PubMed: 5884016]

32. Cuff JA, Barton GJ. Application of multiple sequence alignment profiles to improve protein secondary structure prediction. Proteins 2000;40:502–511. [PubMed: 10861942]

33. Sivaram MV, Furgason ML, Brewer DN, Munson M. The structure of the exocyst subunit Sec6p defines a conserved architecture with diverse roles. Nat Struct Mol Biol 2006;13:555–556. [PubMed: 16699513]

34. Wu S, Mehta SQ, Pichaud F, Bellen HJ, Quiocho FA. Sec15 interacts with Rab11 via a novel domain and affects Rab11 localization in vivo. Nat Struct Mol Biol 2005;12:879–885. [PubMed: 16155582]

35. Munson M, Novick P. The exocyst defrocked, a framework of rods revealed. Nat Struct Mol Biol 2006;13:577–581. [PubMed: 16826234]

36. Berman HM, Westbrook J, Feng Z, Gilliland G, Bhat TN, Weissig H, Shindyalov IN, Bourne PE. The Protein Data Bank. Nucleic Acids Res 2000;28:235–242. [PubMed: 10592235]

37. Holm L, Sander C. Dali: a network tool for protein structure comparison. Trends Biochem Sci 1995;20:478–480. [PubMed: 8578593]

38. Pashkova N, Jin Y, Ramaswamy S, Weisman LS. Structural basis for myosin V discrimination between distinct cargoes. Embo J 2006;25:693–700. [PubMed: 16437158]

39. Otwinowski Z, Minor W. Processing of X-ray Diffraction Data Collected in Oscillation Mode. Methods in Enzymology 1997;276:307–326.

40. Hendrickson WA, Ogata CM. Phase Determination from Multiwavelength Anomalous Diffraction Measurements. Methods in Enzymology 1997;276:494–523.

41. Brunger AT, Adams PD, Clore GM, DeLano WL, Gros P, Grosse-Kunstleve RW, Jiang JS, Kuszewski J, Nilges M, Pannu NS, Read RJ, Rice LM, Simonson T, Warren GL. Crystallography & NMR system: A new software suite for macromolecular structure determination. Acta Crystallogr D Biol Crystallogr 1998;54:905–921. [PubMed: 9757107]

42. Weeks CM, Miller R. Optimizing Shake-and-Bake for proteins. Acta Crystallogr D Biol Crystallogr 1999;55:492–500. [PubMed: 10089361]

43. Vonrhein C, Blanc E, Roversi P, Bricogne G. Automated Structure Solution With autoSHARP. Methods Mol Biol 2006;364:215–230. [PubMed: 17172768]

44. Jones TA, Zou JY, Cowan SW, Kjeldgaard M. Improved methods for building protein models in electron density maps and the location of errors in these models. Acta Crystallogr A 1991;47 (Pt 2): 110–119. [PubMed: 2025413]

45. Holm L, Park J. DaliLite workbench for protein structure comparison. Bioinformatics 2000;16:566–567. [PubMed: 10980157]

46. Thompson JD, Higgins DG, Gibson TJ. CLUSTAL W: improving the sensitivity of progressive multiple sequence alignment through sequence weighting, position-specific gap penalties and weight matrix choice. Nucleic Acids Res 1994;22:4673–4680. [PubMed: 7984417]

47. Baker NA, Sept D, Joseph S, Holst MJ, McCammon JA. Electrostatics of nanosystems: application to microtubules and the ribosome. Proc Natl Acad Sci U S A 2001;98:10037–10041. [PubMed: 11517324]
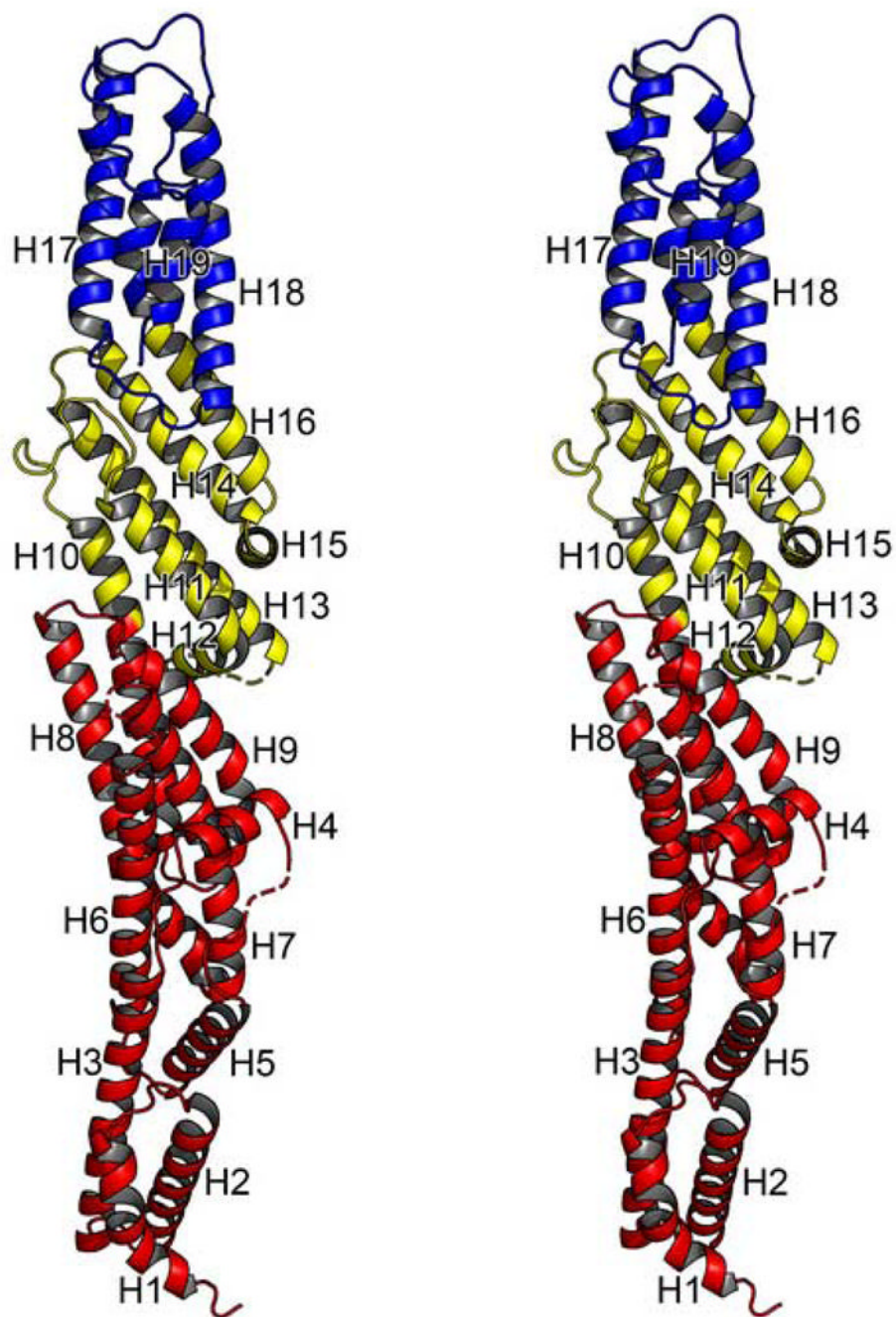
Figure 1. The Structure of Exo70
Stereo cartoon diagram of *Mm*Exo70 is shown. Residues of the N domain are shown in red, M domain in yellow, and C domain in blue. α-helices are drawn as coils and labeled from H1 to H19; turns and loops, solid tubes; unobserved residues, dashed lines (no β strands are observed in the structure).
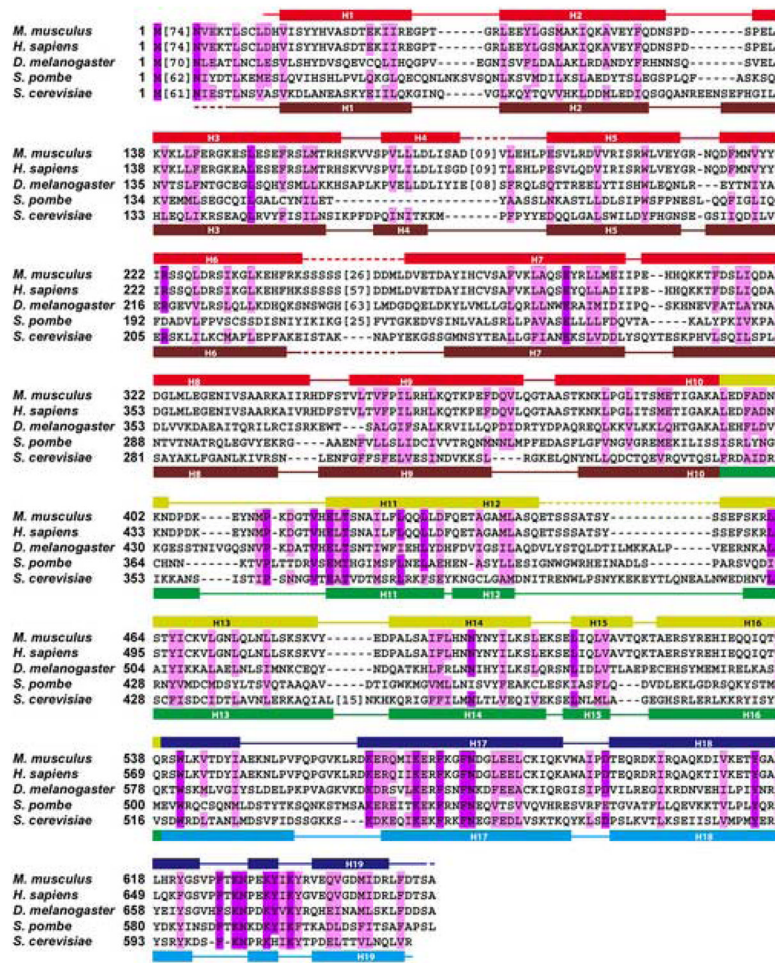
Figure 2. Structural Alignment of Exo70 Proteins
Structural alignment of Exo70 in *M. musculus*, *H. sapiens*, *D. melanogaster*, *S. pombe*, and *S. cerevisiae*. Invariant residues are shaded purple. Similar but not identical residues are shaded pink. Secondary structural elements are indicated above the sequence block for *Mm*Exo70 and below for *Sc*Exo70: α-helices, rectangles; other elements, solid lines; structurally unobserved residues, dashed lines. For *Mm*Exo70, N domain, red; M domain, yellow; and C domain, blue (same as Figure 1). For *Sc*Exo70, N domain, brown; M domain, green; and C domain, cyan. For clarity, sequences lacking homology or unobserved in the structures have been replaced with bracketed numbers indicating the number of residues omitted.
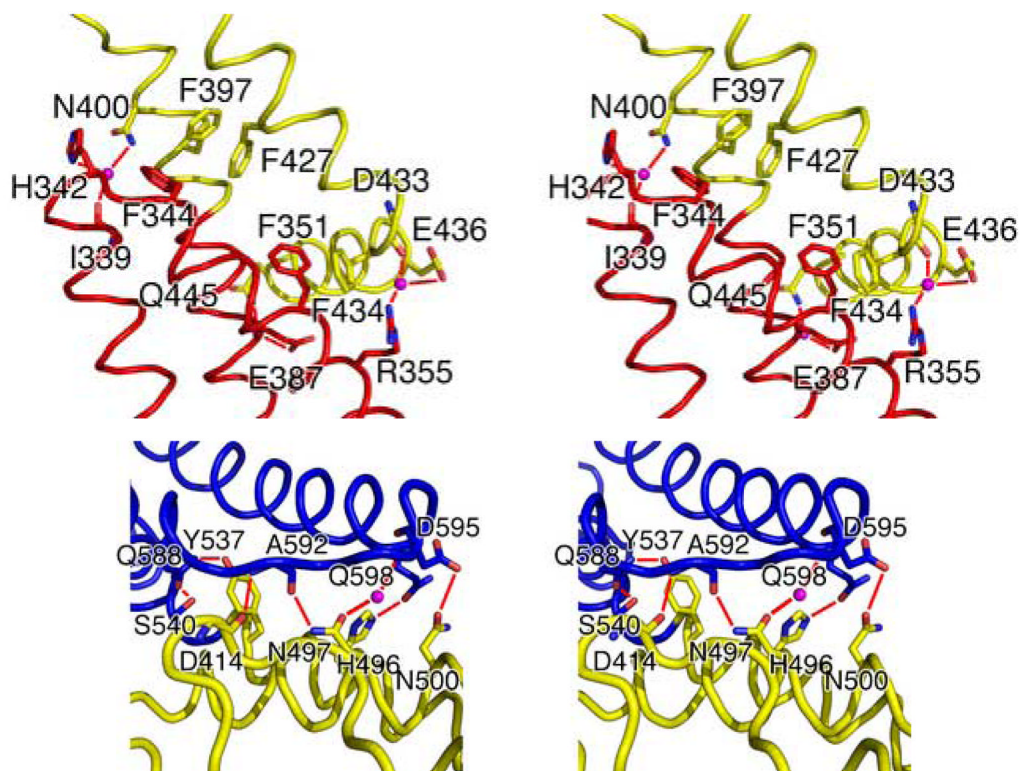
Figure 3. Domain boundaries of *Mm*Exo70
Stereo cartoon diagrams showing interactions between the N and M domains (**A**) and M and C domains (**B**) of *Mm*Exo70. The side chains or main chains of residues involved in domain-domain hydrogen bonds are shown as stick models with oxygen and nitrogen atoms colored red and blue, respectively. The rest of the protein structure is shown as a ribbon drawing and is colored by domain as in Figure 1. Solvent molecules involved in hydrogen bonds are shown as magenta spheres. Hydrogen bonds are depicted as red lines. Aromatic residues involved in the hydrophobic patches are also included in (A). Helices other than H8-H12 are omitted in (A) and H19 is omitted in (B) for clarity.
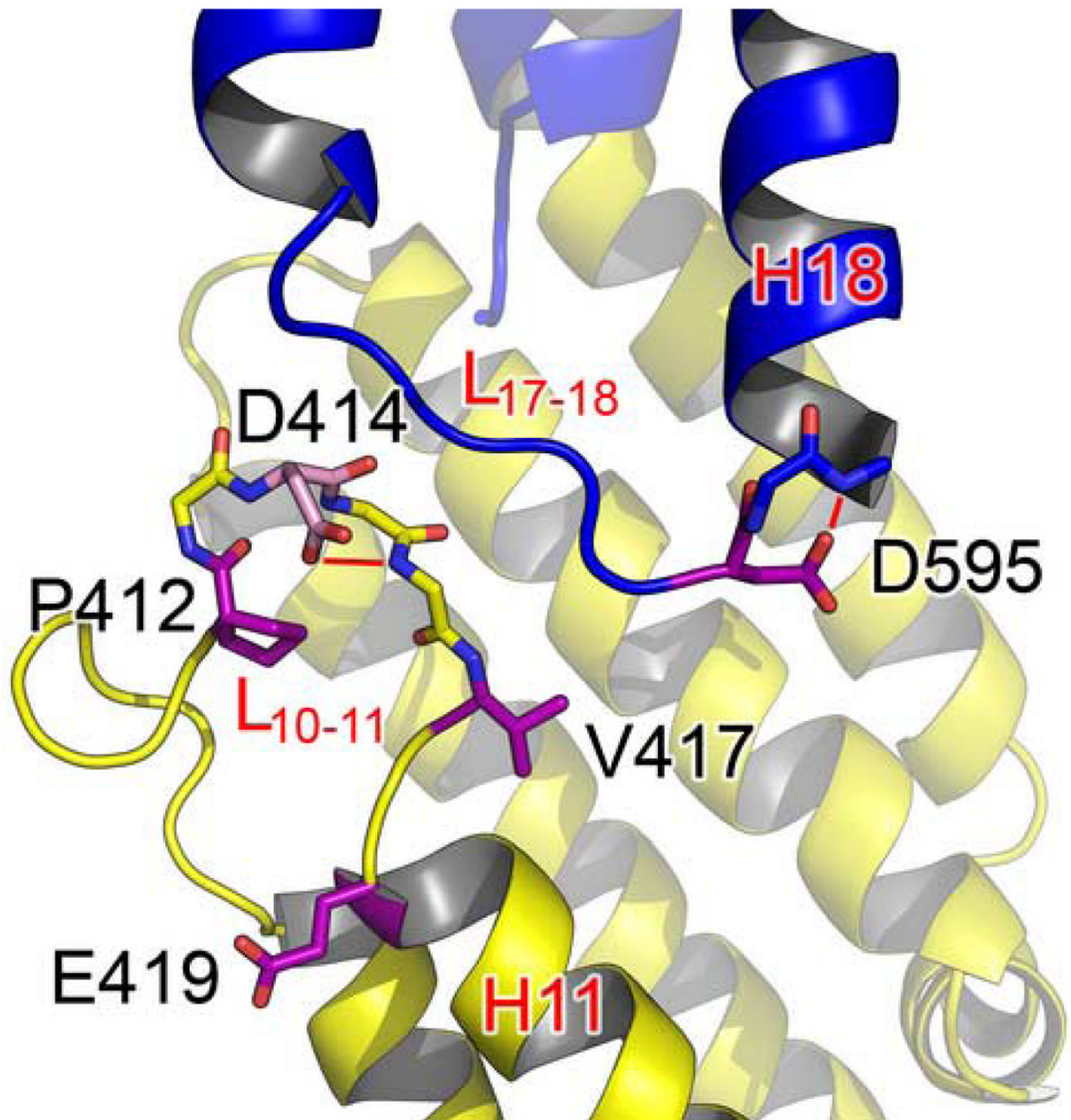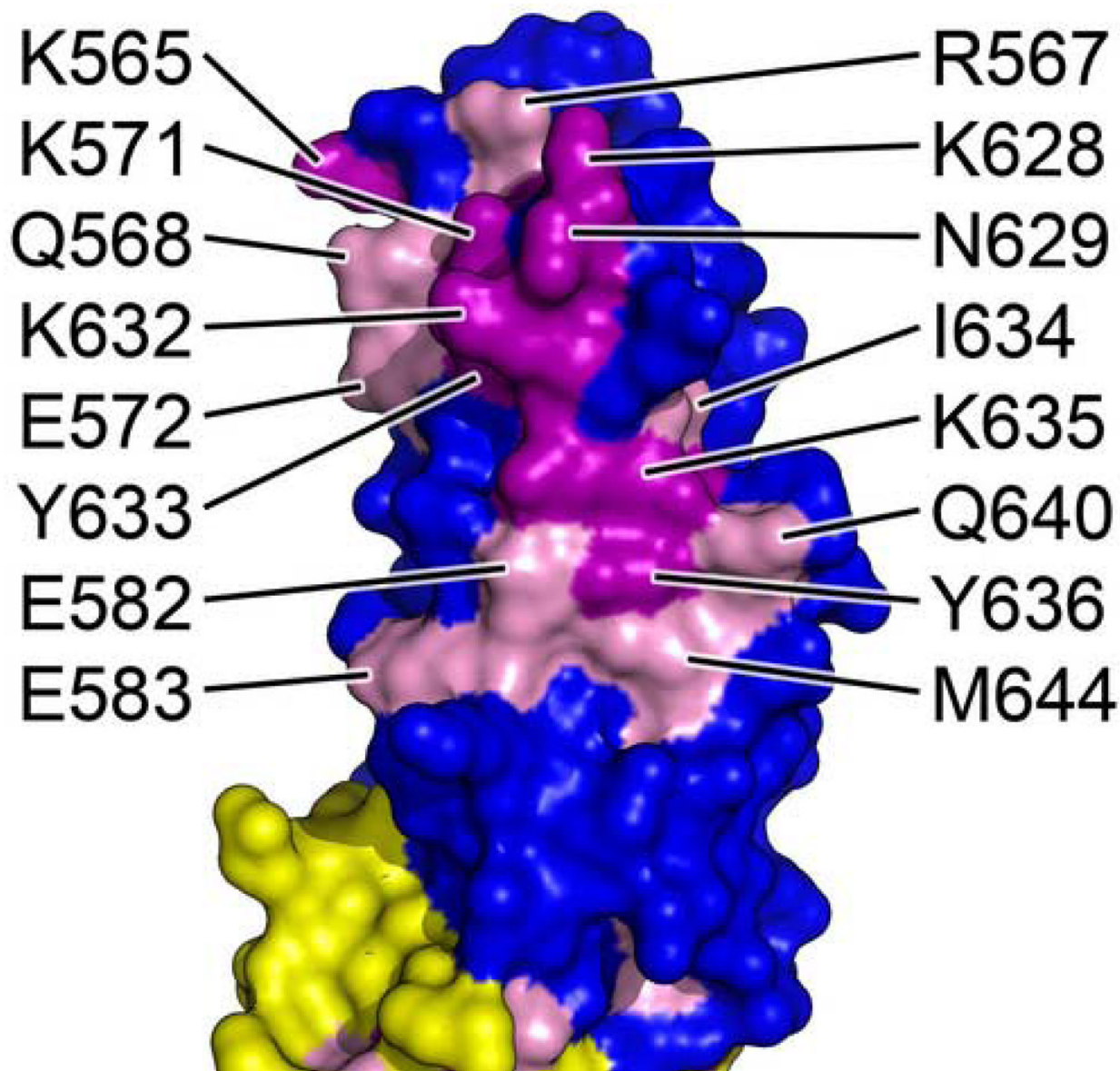
Figure 4. Conserved surface residues of *Mm*Exo70
In both figures, completely conserved residues are colored purple, similar residues are colored pink, and the rest of the molecule is colored by domain as in Figure 1. (**A**) A cartoon diagram of the cluster of conserved residues found on the surface of the M domain of *Mm*Exo70. Main chain atoms are shown for P412-V417 and D595-E597 and side chains are shown for the conserved residues in stick models. Oxygen and nitrogen atoms are colored red and blue, respectively. Hydrogen bonds are depicted as red lines. Relevant α-helices and loops are labeled in red. The view is the same as in Figure 1. (**B**) Molecular surface diagram of the cluster of conserved residues found on the surface of the C domain of *Mm*Exo70. This view is rotated 45° about the long axis from Figure 1.
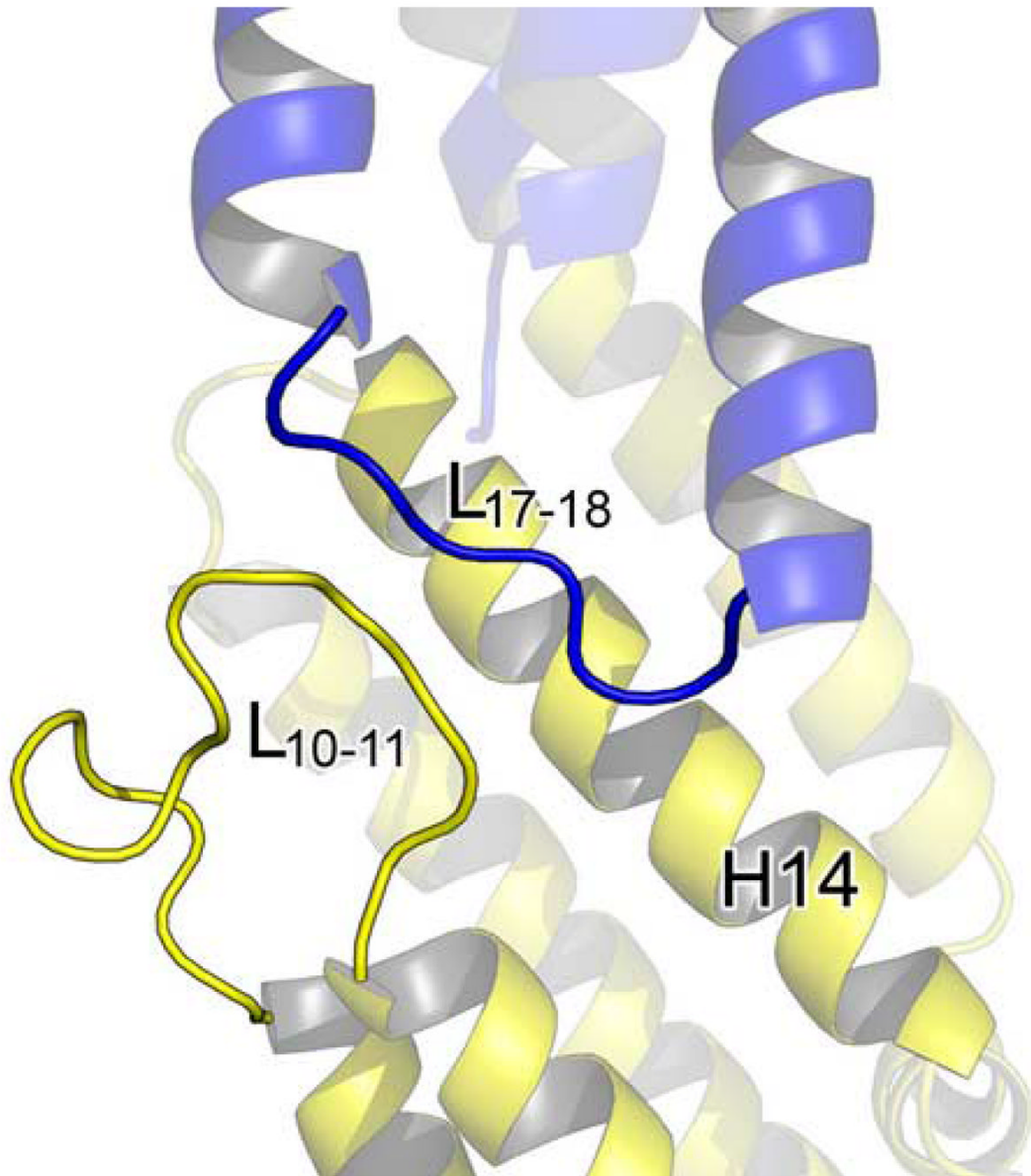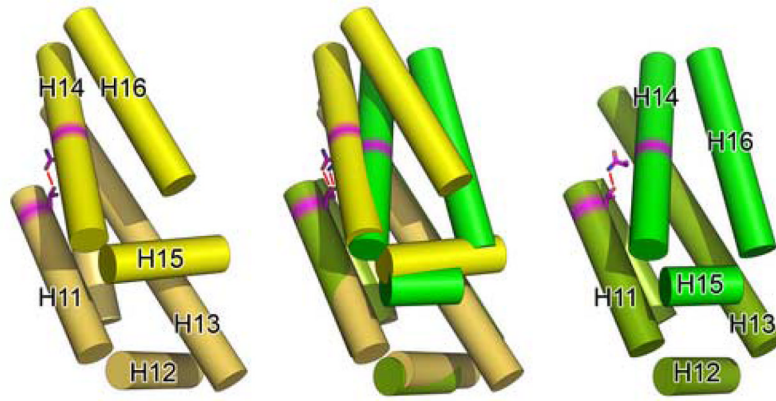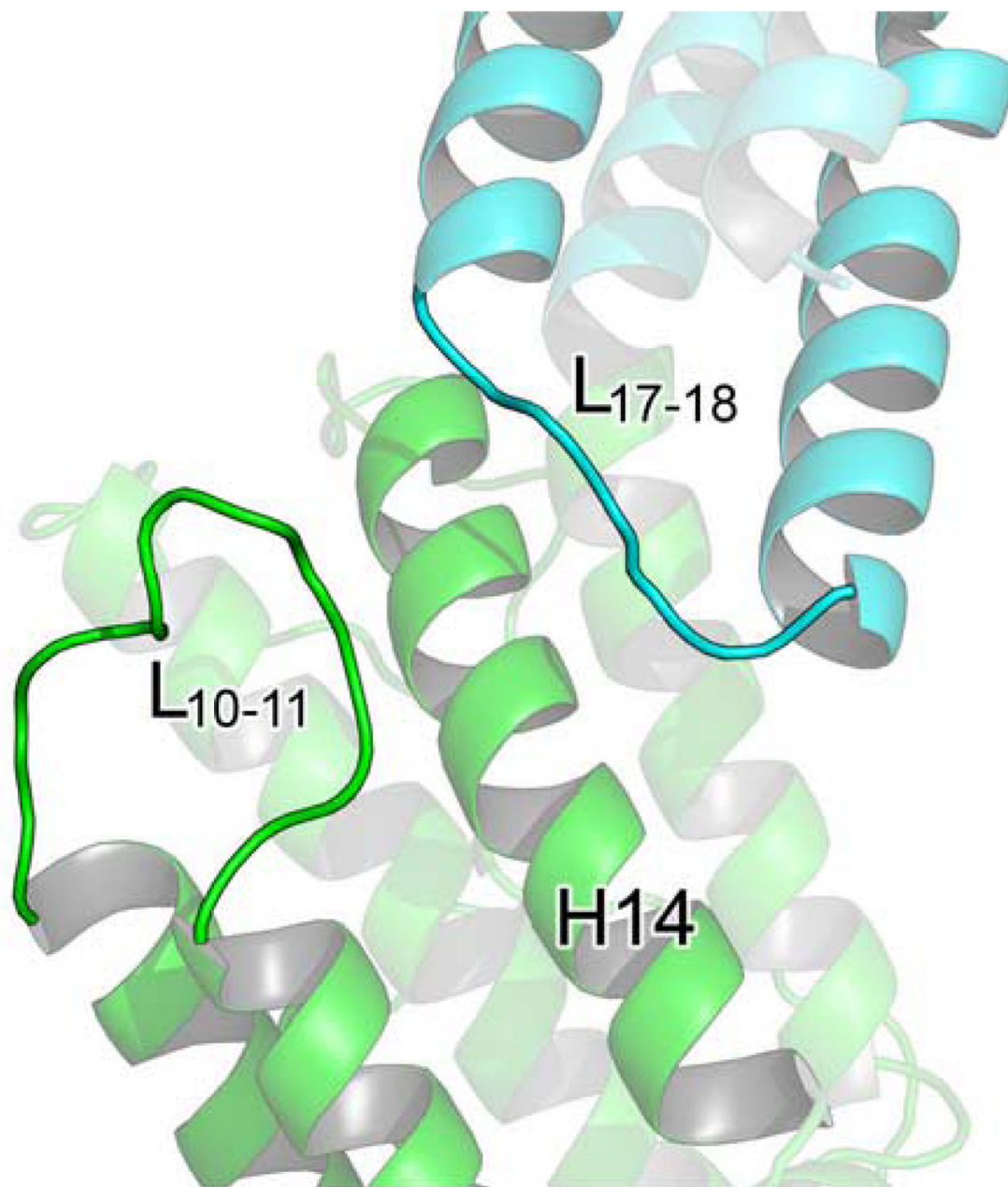
Figure 5. Differences in M domain packing affect M and C domain interactions
(**A**) A cartoon diagram showing the alignment of *Mm*Exo70 with *Sc*Exo70 based on alignment of the N domain. Residues are colored by domain as in Figure 2. (**B**) Schematic diagrams of the M domains of Exo70 with helices shown as cylinders and all loops omitted. The left panel shows *Mm*Exo70 (yellow) and the right panel shows *Sc*Exo70 (green). H11-H16 are labeled. The middle panel shows the alignment of *Mm*Exo70 with *Sc*Exo70 based on H10-H13. The completely conserved hydrogen bond between *Mm*Exo70 Thr421/*Sc*Exo70 Thr372 and *Mm*Exo70 Asn498/*Sc*Exo70 Asn479 is shown as a red line. Note the differences in α-helical packing between the two molecules. (**C**) A cartoon diagram showing the positions of $L_{10–11}$ and $L_{17–18}$ in *Mm*Exo70. Relevant α-helices and loops are labeled. (**D**) A cartoon diagram

showing the positions of L_{10-11} and L_{17-18} in *Sc*Exo70. Relevant α-helices and loops are labeled.
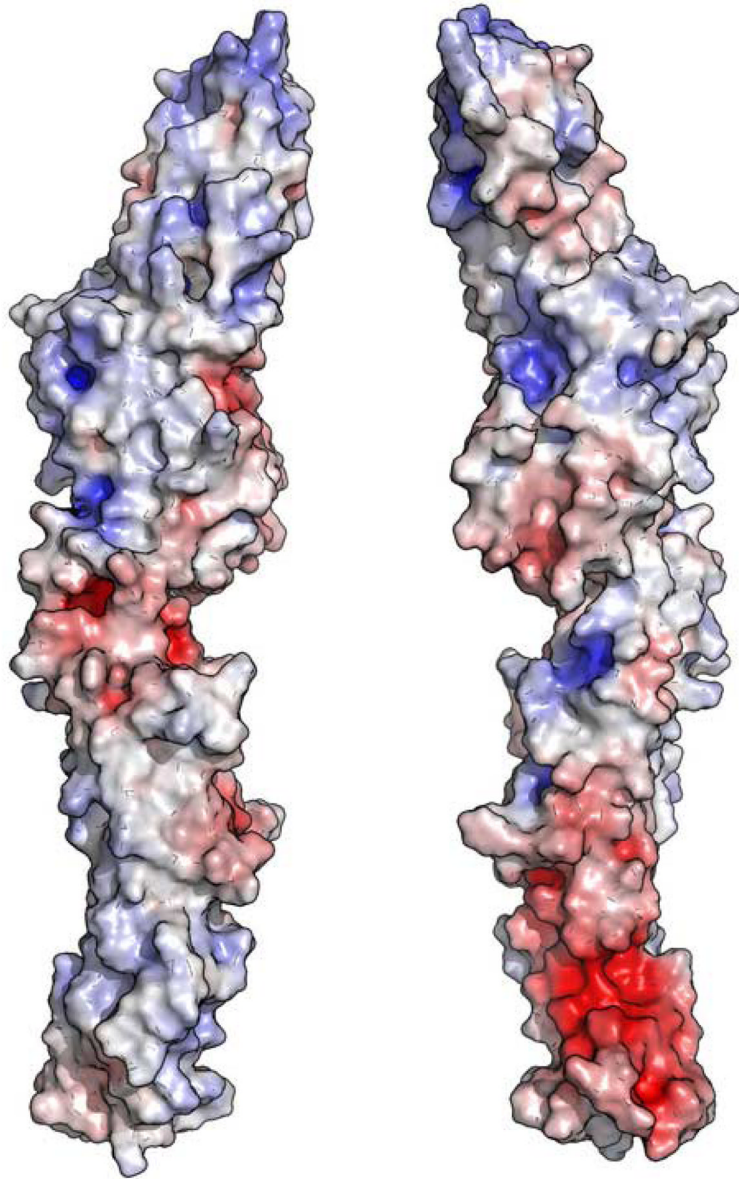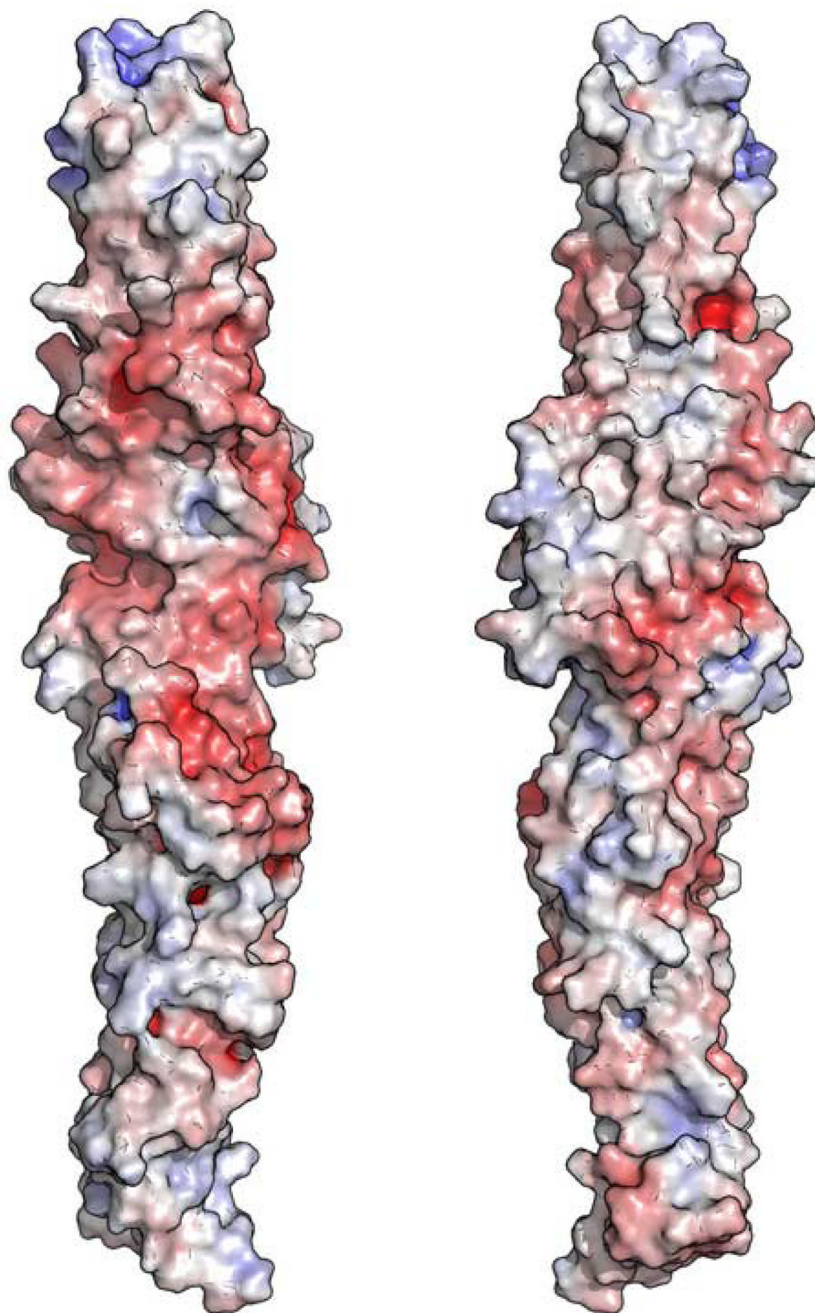
Figure 6. Surface electrostatic potential of Exo70
The molecular surfaces of *Sc*Exo70 (**A**) and *Mm*Exo70 (**B**) are shown. The surfaces are colored on the basis of the solvent-accessible electrostatic potential of the molecules. Blue and red depict positive and negative electrostatic potential, respectively, with a range of $\pm 10 k_B T/e$. Views in the left panels are similar to Figure 1 and are related to the right panels by a 180° rotation about the long axis.
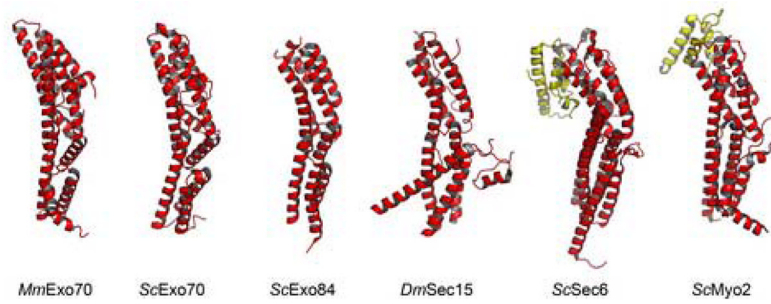
Figure 7. A common fold is found in Exo70, Myo2 and other structures
Cartoon diagrams of molecules containing structures similar to the N domain of *Mm*Exo70. From left to right these are: *Mm*Exo70 N domain, *Sc*Exo70 N domain, *Sc*Exo84 C-terminal domain (PDB ID 2D2S), *Dm*Sec15 C-terminal domain (PDB ID 2A2F), *Sc*Sec6 C-terminal domains (PDB ID 2FJI), and *Sc*Myo2 C-terminal domains (PDB ID 2F6H). Domains common in all these structures are colored red. *Sc*Sec6 and *Sc*Myo2 terminate in a similar three-helix bundle (yellow) not seen in other structures.

Table 1

Crystallographic data statistics for *Mm*Exo70

	*Mm*Exo70 Native	*Mm*Exo70 L-Selenomethionine substituted		
Data collection				
Space group	$P3_221$	$P3_221$		
Cell dimensions [*a*, *b*, *c* (Å)]	61.52, 61.52, 294.73	61.64, 61.64, 294.68		
Resolution (Å)	50.0–2.25 (2.33–2.25)	50.0–2.5 (2.59–2.50)		
		Peak	Inflection	Remote
Wavelength (Å)	0.97926	0.97926	0.97942	0.95660
Completeness (%)	93.7 (77.7)	98.6 (89.2)	97.1 (77.5)	93.4 (59.2)
Redundancy	4.2 (3.1)	6.2 (4.6)	5.7 (3.0)	5.4 (2.3)
$I/\sigma I$	24.6 (3.0)	34.0 (4.7)	32.0 (2.8)	29.8 (1.8)
R_{merge}(%)	5.4 (41.6)	7.9 (29.7)	6.9 (36.5)	6.9 (42.3)
Refinement				
Resolution (Å)	50.0–2.25			
No. reflections in working set	27369			
No. reflections in test set	1435			
R_{work}/R_{free} (%)	23.5/28.5			
No. of atoms				
Protein	4099			
Water	170			
Average *B*-factors				
Protein	54.4			
Water	54.8			
Rms deviations from ideality				
Bond lengths (Å)	0.006			
Bond angles (deg.)	1.1			
Ramachandran plot				
% in most favored regions	92.8			
% in addl. allowed regions	6.5			
% in gen. allowed regions	0.6			

Highest resolution shell shown in parentheses.